This paper is published as part of a PCCP Themed Issue on: Physical Chemistry of Ionic Liquids

Guest Editor: Frank Endres (Technical University of Clausthal, Germany)

Editorial

Physical chemistry of ionic liquids
Phys. Chem. Chem. Phys., 2010, **DOI:** 10.1039/c001176m

Perspectives

Ionicity in ionic liquids: correlation with ionic structure and physicochemical properties
Kazuhide Ueno, Hiroyuki Tokuda and Masayoshi Watanabe, *Phys. Chem. Chem. Phys.*, 2010, **DOI:** 10.1039/b921462n

Design of functional ionic liquids using magneto- and luminescent-active anions
Yukihiro Yoshida and Gunzi Saito, *Phys. Chem. Chem. Phys.*, 2010, **DOI:** 10.1039/b920046k

Accelerating the discovery of biocompatible ionic liquids
Nicola Wood and Gill Stephens, *Phys. Chem. Chem. Phys.*, 2010, **DOI:** 10.1039/b923429b

Ionic liquids and reactions at the electrochemical interface
Douglas R. MacFarlane, Jennifer M. Pringle, Patrick C. Howlett and Maria Forsyth, *Phys. Chem. Chem. Phys.*, 2010, **DOI:** 10.1039/b923053j

Photochemical processes in ionic liquids on ultrafast timescales
Chandrasekhar Nese and Andreas-Neil Unterreiner, *Phys. Chem. Chem. Phys.*, 2010, **DOI:** 10.1039/b916799b

At the interface: solvation and designing ionic liquids
Robert Hayes, Gregory G. Warr and Rob Atkin, *Phys. Chem. Chem. Phys.*, 2010, **DOI:** 10.1039/b920393a

Ionic liquids in surface electrochemistry
Hongtao Liu, Yang Liu and Jinghong Li, *Phys. Chem. Chem. Phys.*, 2010, **DOI:** 10.1039/b921469k

Discussion

Do solvation layers of ionic liquids influence electrochemical reactions?
Frank Endres, Oliver Höfft, Natalia Borisenko, Luiz Henrique Gasparotto, Alexandra Prowald, Rihab Al-Salman, Timo Carstens, Rob Atkin, Andreas Bund and Sherif Zein El Abedin, *Phys. Chem. Chem. Phys.*, 2010, **DOI:** 10.1039/b923527m

Papers

Plasma electrochemistry in ionic liquids: deposition of copper nanoparticles
M. Brettholle, O. Höfft, L. Klarhöfer, S. Mathes, W. Maus-Friedrichs, S. Zein El Abedin, S. Krischok, J. Janek and F. Endres, *Phys. Chem. Chem. Phys.*, 2010, **DOI:** 10.1039/b906567a

Size control and immobilization of gold nanoparticles stabilized in an ionic liquid on glass substrates for plasmonic applications
Tatsuya Kameyama, Yumi Ohno, Takashi Kurimoto, Ken-ichi Okazaki, Taro Uematsu, Susumu Kuwabata and Tsukasa Torimoto, *Phys. Chem. Chem. Phys.*, 2010, **DOI:** 10.1039/b914230d

Electrostatic properties of liquid 1,3-dimethylimidazolium chloride: role of local polarization and effect of the bulk
C. Krekeler, F. Dommert, J. Schmidt, Y. Y. Zhao, C. Holm, R. Berger and L. Delle Site, *Phys. Chem. Chem. Phys.*, 2010, **DOI:** 10.1039/b917803c

Selective removal of acetylenes from olefin mixtures through specific physicochemical interactions of ionic liquids with acetylenes
Jung Min Lee, Jelliarko Palgunadi, Jin Hyung Kim, Srun Jung, Young-seop Choi, Minserk Cheong and Hoon Sik Kim, *Phys. Chem. Chem. Phys.*, 2010, **DOI:** 10.1039/b915989d

Screening of pairs of ions dissolved in ionic liquids
R. M. Lynden-Bell, *Phys. Chem. Chem. Phys.*, 2010, **DOI:** 10.1039/b916987c

Double layer, diluent and anode effects upon the electrodeposition of aluminium from chloroaluminate based ionic liquids
Andrew P. Abbott, Fulian Qiu, Hadi M. A. Abood, M. Rostom Ali and Karl S. Ryder, *Phys. Chem. Chem. Phys.*, 2010, **DOI:** 10.1039/b917351j

A comparison of the cyclic voltammetry of the Sn/Sn(II) couple in the room temperature ionic liquids *N*-butyl-*N*-methylpyrrolidinium dicyanamide and *N*-butyl-*N*-methylpyrrolidinium bis(trifluoromethylsulfonyl)imide: solvent induced changes of electrode reaction mechanism
Benjamin C. M. Martindale, Sarah E. Ward Jones and Richard G. Compton, *Phys. Chem. Chem. Phys.*, 2010, **DOI:** 10.1039/b920217j

Ionic liquids through the looking glass: theory mirrors experiment and provides further insight into aromatic substitution processes
Shon Glyn Jones, Hon Man Yau, Erika Davies, James M. Hook, Tristan G. A. Youngs, Jason B. Harper and Anna K. Croft, *Phys. Chem. Chem. Phys.*, 2010, **DOI:** 10.1039/b919831h

Nitrile-functionalized pyrrolidinium ionic liquids as solvents for cross-coupling reactions involving *in situ* generated nanoparticle catalyst reservoirs
Yugang Cui, Ilaria Biondi, Manish Chaubey, Xue Yang, Zhaofu Fei, Rosario Scopelliti, Christian G. Hartinger, Yongdan Li, Cinzia Chiappe and Paul J. Dyson, *Phys. Chem. Chem. Phys.*, 2010, **DOI:** 10.1039/b920025h

Ionic liquid as plasticizer for europium(III)-doped luminescent poly(methyl methacrylate) films
Kyra Lunstroot, Kris Driesen, Peter Nockemann, Lydie Viau, P. Hubert Mutin, André Vioux and Koen Binnemans, *Phys. Chem. Chem. Phys.*, 2010, **DOI:** 10.1039/b920145a

***Ab initio* study on S_N2 reaction of methyl *p*-nitrobenzenesulfonate and chloride anion in [mmim][PF_6]**
Seigo Hayaki, Kentaro Kido, Hirofumi Sato and Shigeyoshi Sakaki, *Phys. Chem. Chem. Phys.*, 2010, **DOI:** 10.1039/b920190b

Influence of imidazolium bis(trifluoromethylsulfonylimide)s on the rotation of spin probes comprising ionic and hydrogen bonding groups
Veronika Strehmel, Hans Rexhausen and Peter Strauch, *Phys. Chem. Chem. Phys.*, 2010, **DOI:** 10.1039/b920586a

Thermo-solvatochromism in binary mixtures of water and ionic liquids: on the relative importance of solvophobic interactions
Bruno M. Sato, Carolina G. de Oliveira, Clarissa T. Martins and Omar A. El Seoud, *Phys. Chem. Chem. Phys.*, 2010, **DOI:** 10.1039/b921391k

Patterns of protein unfolding and protein aggregation in ionic liquids
Diana Constatinescu, Christian Herrmann and Hermann Weingärtner, *Phys. Chem. Chem. Phys.*, 2010,
DOI: 10.1039/b921037g

High vacuum distillation of ionic liquids and separation of ionic liquid mixtures
Alasdair W. Taylor, Kevin R. J. Lovelock, Alexey Deyko, Peter Licence and Robert G. Jones, *Phys. Chem. Chem. Phys.*, 2010,
DOI: 10.1039/b920931j

Designer molecular probes for phosphonium ionic liquids
Robert Byrne, Simon Coleman, Simon Gallagher and Dermot Diamond, *Phys. Chem. Chem. Phys.*, 2010,
DOI: 10.1039/b920580b

States and migration of an excess electron in a pyridinium-based, room-temperature ionic liquid: an *ab initio* molecular dynamics simulation exploration
Zhiping Wang, Liang Zhang, Robert I. Cukier and Yuxiang Bu, *Phys. Chem. Chem. Phys.*, 2010, **DOI:** 10.1039/b921104g

J-aggregation of ionic liquid solutions of *meso*-tetrakis(4-sulfonatophenyl)porphyrin
Maroof Ali, Vinod Kumar, Sheila N. Baker, Gary A. Baker and Siddharth Pandey, *Phys. Chem. Chem. Phys.*, 2010,
DOI: 10.1039/b920500d

Spontaneous product segregation from reactions in ionic liquids: application in Pd-catalyzed aliphatic alcohol oxidation
Charlie Van Doorslaer, Yves Schellekens, Pascal Mertens, Koen Binnemans and Dirk De Vos, *Phys. Chem. Chem. Phys.*, 2010,
DOI: 10.1039/b920813p

Electrostatic interactions in ionic liquids: the dangers of dipole and dielectric descriptions
Mark N. Kobrak and Hualin Li, *Phys. Chem. Chem. Phys.*, 2010,
DOI: 10.1039/b920080k

Insights into the surface composition and enrichment effects of ionic liquids and ionic liquid mixtures
F. Maier, T. Cremer, C. Kolbeck, K. R. J. Lovelock, N. Paape, P. S. Schulz, P. Wasserscheid and H.-P. Steinrück, *Phys. Chem. Chem. Phys.*, 2010, **DOI:** 10.1039/b920804f

Ionic liquids and reactive azeotropes: the continuity of the aprotic and protic classes
José N. Canongia Lopes and Luís Paulo N. Rebelo, *Phys. Chem. Chem. Phys.*, 2010, **DOI:** 10.1039/b922524m

A COSMO-RS based guide to analyze/quantify the polarity of ionic liquids and their mixtures with organic cosolvents
José Palomar, José S. Torrecilla, Jesús Lemus, Víctor R. Ferro and Francisco Rodríguez, *Phys. Chem. Chem. Phys.*, 2010,
DOI: 10.1039/b920651p

Solid and liquid charge-transfer complex formation between 1-methylnaphthalene and 1-alkyl-cyanopyridinium bis{(trifluoromethyl)sulfonyl}imide ionic liquids
Christopher Hardacre, John D. Holbrey, Claire L. Mullan, Mark Nieuwenhuyzen, Tristan G. A. Youngs, Daniel T. Bowron and Simon J. Teat, *Phys. Chem. Chem. Phys.*, 2010,
DOI: 10.1039/b921160h

Blending ionic liquids: how physico-chemical properties change
F. Castiglione, G. Raos, G. Battista Appetecchi, M. Montanino, S. Passerini, M. Moreno, A. Famulari and A. Mele, *Phys. Chem. Chem. Phys.*, 2010, **DOI:** 10.1039/b921816e

NMR spectroscopic studies of cellobiose solvation in EmimAc aimed to understand the dissolution mechanism of cellulose in ionic liquids
Jinming Zhang, Hao Zhang, Jin Wu, Jun Zhang, Jiasong He and Junfeng Xiang, *Phys. Chem. Chem. Phys.*, 2010,
DOI: 10.1039/b920446f

Electrochemical carboxylation of α-chloroethylbenzene in ionic liquids compressed with carbon dioxide
Yusuke Hiejima, Masahiro Hayashi, Akihiro Uda, Seiko Oya, Hiroyuki Kondo, Hisanori Senboku and Kenji Takahashi, *Phys. Chem. Chem. Phys.*, 2010, **DOI:** 10.1039/b920413j

A theoretical study of the copper(I)-catalyzed 1,3-dipolar cycloaddition reaction in dabco-based ionic liquids: the anion effect on regioselectivity
Cinzia Chiappe, Benedetta Mennucci, Christian Silvio Pomelli, Angelo Sanzone and Alberto Marra, *Phys. Chem. Chem. Phys.*, 2010, **DOI:** 10.1039/b921204c

Fragility, Stokes–Einstein violation, and correlated local excitations in a coarse-grained model of an ionic liquid
Daun Jeong, M. Y. Choi, Hyung J. Kim and YounJoon Jung, *Phys. Chem. Chem. Phys.*, 2010, **DOI:** 10.1039/b921725h

Reactions of excited-state benzophenone ketyl radical in a room-temperature ionic liquid
Kenji Takahashi, Hiroaki Tezuka, Shingo Kitamura, Toshifumi Satoh and Ryuzi Katoh, *Phys. Chem. Chem. Phys.*, 2010,
DOI: 10.1039/b920131a

In search of pure liquid salt forms of aspirin: ionic liquid approaches with acetylsalicylic acid and salicylic acid
Katharina Bica, Christiaan Rijksen, Mark Nieuwenhuyzen and Robin D. Rogers, *Phys. Chem. Chem. Phys.*, 2010,
DOI: 10.1039/b923855g

Nanocomposites of ionic liquids confined in mesoporous silica gels: preparation, characterization and performance
Juan Zhang, Qinghua Zhang, Xueli Li, Shimin Liu, Yubo Ma, Feng Shi and Youquan Deng, *Phys. Chem. Chem. Phys.*, 2010,
DOI: 10.1039/b920556j

An ultra high vacuum-spectroelectrochemical study of the dissolution of copper in the ionic liquid (*N*-methylacetate)-4-picolinium bis(trifluoromethylsulfonyl)imide
Fulian Qiu, Alasdair W. Taylor, Shuang Men, Ignacio J. Villar-Garcia and Peter Licence, *Phys. Chem. Chem. Phys.*, 2010,
DOI: 10.1039/b924985k

Understanding siloxane functionalised ionic liquids
Heiko Niedermeyer, Mohd Azri Ab Rani, Paul D. Lickiss, Jason P. Hallett, Tom Welton, Andrew J. P. White and Patricia A. Hunt, *Phys. Chem. Chem. Phys.*, 2010, **DOI:** 10.1039/b922011a

On the electrodeposition of tantalum from three different ionic liquids with the bis(trifluoromethyl sulfonyl) amide anion
Adriana Ispas, Barbara Adolphi, Andreas Bund and Frank Endres, *Phys. Chem. Chem. Phys.*, 2010,
DOI: 10.1039/b922071m

Solid-state dye-sensitized solar cells using polymerized ionic liquid electrolyte with platinum-free counter electrode
Ryuji Kawano, Toru Katakabe, Hironobu Shimosawa, Md. Khaja Nazeeruddin, Michael Grätzel, Hiroshi Matsui, Takayuki Kitamura, Nobuo Tanabec and Masayoshi Watanabe, *Phys. Chem. Chem. Phys.*, 2010, **DOI:** 10.1039/b920633g

Dynamics of ionic liquid mediated quantised charging of monolayer-protected clusters
Stijn F. L. Mertens, Gábor Mészáros and Thomas Wandlowski, *Phys. Chem. Chem. Phys.*, 2010, **DOI:** 10.1039/b921368f

Ionic liquids and solids with paramagnetic anions†‡

Brenna M. Krieger,[a] Heather Y. Lee,[a] Thomas J. Emge,[a] James F. Wishart[b] and Edward W. Castner, Jr.[a]

Received 2nd October 2009, Accepted 23rd April 2010
DOI: 10.1039/b920652n

Four paramagnetic ionic compounds have been prepared and their magnetic, structural and thermal properties have been investigated. The four compounds are methylbutylpyrrolidinium tetrachloroferrate(III) ($[Pyrr_{14}]^+/[FeCl_4]^-$), methyltributylammonium tetrachloroferrate(III) ($[N_{1444}]^+/[FeCl_4]^-$), butylmethylimidazolium tetrachloroferrate(III) ($[bmim]^+/[FeCl_4]^-$) and tetrabutylammonium bromotrichloroferrate(III) ($[N_{4444}]^+/[FeBrCl_3]^-$). Temperature-dependent studies of their magnetic behaviors show that all four compounds are paramagnetic at ambient temperatures. Glass transitions are observed for only two of the four compounds, $[Pyrr_{14}]^+/[FeCl_4]^-$ and $[bmim]^+/[FeCl_4]^-$. Crystal structures for $[Pyrr_{14}]^+/[FeCl_4]^-$ and $[N_{1444}]^+/[FeCl_4]^-$ are compared with the previously reported $[N_{4444}]^+/[FeBrCl_3]^-$.

Introduction

Ionic liquids (ILs) are commonly defined as molten salts with melting temperatures below 100 °C. The chemical and physical properties of ILs vary widely depending on their compositions, but in general they have wider electrochemical windows and lower vapor pressures than conventional organic solvents.[1] The exponential growth of interest in ILs and their remarkable properties during the previous decade has also stimulated investigations into related ionic solids having melting points above 100 °C.

Fluids with macroscopic paramagnetic or ferromagnetic responses have been created using several methods. One method involves dissolving or suspending paramagnetic or ferromagnetic particles in a solvent. Magnetorheological fluids are normally made by dispersing magnetic particles (such as iron oxides) in a carrier fluid, which then permits control of the bulk viscosity by external magnetic fields.[2] A parallel application is the stirring of non-magnetic particles by the rotation induced in a paramagnetic ionic liquid, $[bmim]^+/[FeCl_4]^-$, as it responds to a rotating external magnetic field.[3] In a related manner, paramagnetic γ-Fe_2O_3 and $CoFe_2O_4$ nanoparticles can be added to non-magnetic ionic liquids to create a paramagnetic fluid.[4] The synthesis of molecular magnets, including cyano-bridged magnetic nanoparticles, can be optimized by using ionic liquids as the reaction solvent.[5] Catalytic processes such as aryl Grignard cross-coupling reactions[6] and Friedel–Crafts reactions in mesoporous silica[7] have been enhanced by replacing the traditional $FeCl_3$ catalyst by ionic liquid catalysts such as $[bmim]^+/[FeCl_4]^-$.

Paramagnetic ionic liquids based on anions comprising transition-metal coordination complexes have been reported by several research groups. Fe(III)-containing ILs are especially interesting because of their paramagnetic nature that combines the properties of conventional ferrofluids with those of ILs. Paramagnetic ILs having anions based on iron-gallium[8] or iron[9] were reported by Yoshida, *et al.* Hamaguchi and coworkers have published several articles on the $[bmim]^+/[FeCl_4]^-$ paramagnetic IL.[10–13] Abbott, *et al.* reported ionic liquids with the $[FeCl_4]^-$ anion paired with both trimethylethanolammonium and dimethylphenylethanolammonium cations.[14] Several other ionic solids based on the $[FeCl_4]^-$ anion have been reported with melting temperatures just above 100 °C.[15–17] Del Sesto *et al.* have reported a series of paramagnetic ionic liquids having tetraalkylphosphonium or alkylmethylimidazolium cations paired with tetrahedral or octahedral symmetry transition metal anions, for which the metal is iron, cobalt, manganese or gadolinium.[18] Kozlova, *et al.* reported a paramagnetic ionic liquid with an anion containing Co(II), $([bmim]^+)_2/[CoBr_4]^{2-}$.[19] Mudring and coworkers have prepared and characterized paramagnetic ionic liquids with transition metals and lanthanides.[20,21] Although the higher spin moments of certain *f*-block elements can produce ionic liquids with stronger magnetism, the low cost and relative abundance of iron make Fe-based magnetic ILs attractive subjects for continued study.

To further investigate the thermal and structural properties of paramagnetic ionic compounds, two new paramagnetic ionic species have been synthesized and characterized: methylbutylpyrrolidinium tetrachloroferrate(III) ($[Pyrr_{14}]^+/[FeCl_4]^-$) and methyltributylammonium tetrachloroferrate(III) ($[N_{1444}]^+/[FeCl_4]^-$). The properties of the two new compounds will be compared with two previously reported ionic compounds, tetrabutylammonium bromotrichloroferrate(III) ($[N_{4444}]^+/[FeBrCl_3]^-$) and butylmethylimidazolium tetrachloroferrate(III) ($[bmim]^+/[FeCl_4]^-$). The four paramagnetic ionic compounds reported herein are shown in Fig. 1. Crystallographic data are reported for our two new compounds $[Pyrr_{14}]^+/[FeCl_4]^-$ and $[N_{1444}]^+/[FeCl_4]^-$. These structures are compared with the

[a] *Department of Chemistry and Chemical Biology Rutgers, The State University of New Jersey, Piscataway, NJ 08854-8087*
[b] *Chemistry Department, Brookhaven National Laboratory, Upton, NY 11973-5000*

† Electronic supplementary information (ESI) available: Experimental details. CCDC reference numbers 781604–781605. For ESI and crystallographic data in CIF or other electronic format see DOI: 10.1039/b920652n

‡ This article was submitted as part of a Themed Issue on ionic liquids. Other papers on this topic can be found in issue 8 of vol. 12 (2010). This issue can be found from the *PCCP* homepage [http://www.rsc.org/pccp]

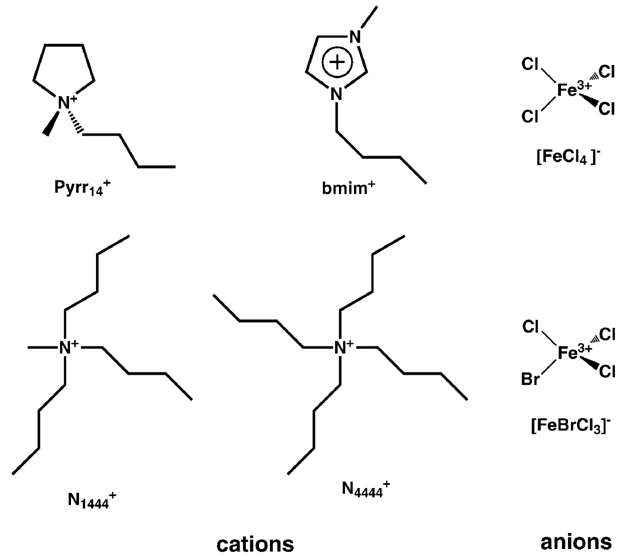

Fig. 1 Paramagnetic ionic liquids and solids.

structure of $[N_{4444}]^+/[FeBrCl_3]^-$ that was reported by Kruszyński and Wyrzykowski.[22] The magnetic properties of each compound were characterized with a magnetometer.

Experimental methods

Synthesis: new ionic compounds

Microwave syntheses were done using a CEM Discover reactor. Reagents were obtained from several sources: 1-methylpyrrolidine (99%), acetonitrile (99.9%), $FeCl_3 \cdot 6H_2O$ (97%), anhydrous 1-chlorobutane (99.5%), anhydrous ethyl acetate (99.8%), anhydrous ethyl ether (99%) and methyltributylammonium chloride (98%) were purchased from Sigma-Aldrich, Inc. HCl (37%) was purchased from Mallinckrodt Chemical, 1-chlorobutane from Eastman and ethanol (200 proof) from Pharmaco. All reagents were used as received without further purification.

Each of the four final products was dried in vacuum at 343–353 K for at least 24 h. to remove remaining solvent or water. Parent *m*/*z* ratios for both the cation and anion were confirmed using a Thermo Finnigan model LCQ Advantage electrospray ionization mass spectrometer. Recrystallization to produce crystals for X-ray diffraction was done in methanol by making a supersaturated solution at 325–345 K and allowing it to gradually cool at room temperature.

$[Pyrr_{14}]^+/[FeCl_4]^-$. $[Pyrr_{14}]^+/[FeCl_4]^-$ was synthesized by metathesis of methylbutylpyrrolidinium chloride ($[Pyrr_{14}]^+/[Cl]^-$) with $FeCl_3 \cdot 6H_2O$ using a similar method to the one previously reported by Evans *et al.*[23] $[Pyrr_{14}]^+/[Cl]^-$ was prepared *via* microwave synthesis as follows. 1-methylpyrrolidine (141 mmol) and 1-chlorobutane (158 mmol) were mixed in a 80 ml microwave vessel with acetonitrile (153 mmol) as solvent. Reaction conditions used were: power 60 watt; temperature ramp 1 min; hold 20 min; 140 °C reaction temperature; maximum pressure set to 10.0 bar. The white precipitate product was filtered and washed with anhydrous ethyl ether. An 82% yield of $[Pyrr_{14}]^+/[Cl]^-$ resulted. For the metathesis of $[Pyrr_{14}]^+/[Cl]^-$ with $FeCl_3 \cdot 6H_2O$, $FeCl_3 \cdot 6H_2O$ (9.99 mmol) was first dissolved in 37% HCl (3.29×10^3 mmol). Precipitation of $[Pyrr_{14}]^+/[FeCl_4]^-$ occurred instantly on addition of $[Pyrr_{14}]^+/[Cl]^-$ (124 mmol). The $[Pyrr_{14}]^+/[FeCl_4]^-$ precipitate was filtered and washed with cold ethyl acetate. The yield for $[Pyrr_{14}]^+/[FeCl_4]^-$ was 76%.

$[N_{1444}]^+/[FeCl_4]^-$. $[N_{1444}]^+/[FeCl_4]^-$ was synthesized by a method similar to that described by Hay *et al.* for the preparation of $[N_{4444}]^+/[FeCl_4]^-$.[24] $FeCl_3 \cdot 6H_2O$ (9.99 mmol) was dissolved in 37% HCl (3290 mmol) after which methyltributylammonium chloride (136 mmol) was added to the yellow solution while stirring. The $[N_{1444}]^+/[FeCl_4]^-$ precipitate was filtered and washed with dry ethanol. The product yield was 91%.

Preparation of other ionic compounds

$[N_{4444}]^+/[FeBrCl_3]^-$ and $[bmim]^+/[FeCl_4]^-$. $[N_{4444}]^+/[FeBrCl_3]^-$ was prepared using the method reported by Kruszyński and Wyrzykowski.[22] The room-temperature IL $[bmim]^+/[FeCl_4]^-$ was synthesized using a procedure previously reported by Hayashi, *et al.*[10]

X-Ray structure determination

X-ray diffraction data for $[N_{1444}]^+/[FeCl_4]^-$ and $[Pyrr_{14}]^+/[FeCl_4]^-$ crystals were collected using a Bruker Smart APEX CCD diffractometer with graphite-monochromatized Mo Kα radiation (λ = 0.71073 Å). For each structure, a crystal of approximately 0.0024 to 0.0027 mm^3 volume was immersed in Paratone-N oil and held at 100 K. The data were corrected for Lorentz and polarization effects and for absorption, the latter by using a multiscan (SADABS) method.[25] The structure was solved by direct methods (SHELXS86).[26] All non-hydrogen atoms were refined (SHELXL97) based on F_{obs}^2.[26] Crystallographic data and final R indices for $[N_{1444}]^+/[FeCl_4]^-$ and $[Pyrr_{14}]^+/[FeCl_4]^-$ are summarized in Table 1; full crystallographic information is provided in the Crystallographic Information File appended to the Supplementary Information.

Vibrational spectroscopy

Ambient room temperature (294 ± 1 K) Raman spectroscopy was performed using a Renishaw System 1000 dispersive micro-Raman spectrometer. The system has a 786 nm diode laser for sample illumination with a 1 cm^{-1} resolution and a Peltier-cooled CCD detector. The ambient temperature FT-IR and Raman spectra are shown in the Supplementary Information.

Thermal measurements

Differential scanning calorimetry (DSC) scans for $[bmim]^+/[FeCl_4]^-$, $[Pyrr_{14}]^+/[FeCl_4]^-$ and $[N_{1444}]^+/[FeCl_4]^-$ were taken using a LNCS-cooled TA Q100 DSC instrument. A Perkin-Elmer Pyris 1 DSC Q200 with DX instrument controllers with a nitrogen-purged sample chamber was used for $[N_{4444}]^+/[FeBrCl_3]^-$. Both instruments were pre-cooled and set at a heating/cooling rate of either 5 or 10 K/min with at least two thermal cycles. Transition temperatures were determined using 4–10 mg samples. Samples for DSC experiments were

Table 1 Crystallographic data for $[N_{1444}]^+/[FeCl_4]^-$ and $[Pyrr_{14}]^+/[FeCl_4]^-$ measured at 100 K

Compound	$[Pyrr_{14}]^+/[FeCl_4]^-$	$[N_{1444}]^+/[FeCl_4]^-$
Empirical formula	$C_{12}H_{24}Cl_4FeN$	$C_{13}H_{30}Cl_4FeN$
Formula weight	379.97	398.03
Crystal system	Hexagonal	Orthorhombic
Space group	$P6_3mc$	$Pca2_1$
a (Å)	8.223(1)	15.366(2)
b (Å)	8.223(1)	14.861(2)
c (Å)	13.030(2)	17.361(3)
α (deg)	90	90
β (deg)	90	90
γ (deg)	120	90
Cell volume (Å^3)	763.0(2)	3964.2(11)
Z	2	8
D_{calcd} (Mg m^{-3})	1.654	1.334
Abs coeff (mm^{-1})	1.671	1.289
F(000)	394	1672
No. Obs. reflections ($I > 2\sigma(I)$)	573	11939
Goodness-of-fit on F^2	1.096	1.002
Data/restraints/parameters	573/24/34	11939/229/52
Final R indices (Obs. data)	$R_1 = 0.0978$, $wR_2 = 0.2643$	$R_1 = 0.0393$, $wR_2 = 0.0854$
Final R indices (All data)	$R_1 = 0.1013$, $wR_2 = 0.2690$	$R_1 = 0.0488$, $wR_2 = 0.0896$

prepared under ambient conditions except for the $[bmim]^+/[FeCl_4]^-$ sample, which was prepared in a nitrogen glove box.

Magnetic properties

Temperature-dependent magnetic susceptibility (χ) measurements were made with a Quantum Design MPMS SQUID magnetometer. The magnetic susceptibilities of the samples were measured at a heating/cooling rate of 5 K/min, in an applied field of 1000 gauss and in the temperature range 5 to 350 K for $[N_{1444}]^+/[FeCl_4]^-$ and 5 to 400 K for $[N_{4444}]^+/[FeBrCl_3]^-$ and $[Pyrr_{14}]^+/[FeCl_4]^-$. Before conducting the susceptibility measurement, the samples were cooled from room temperature in the absence of external field. The temperature was read out by thermal diodes to an accuracy of ± 1 K. The samples were loaded into 0.13 mL Torpac gelatin capsules and the sample chamber was evacuated prior to measurement. The effective magnetic moment was calculated by the equation, $\mu_{eff} = \mu_B\sqrt{8C}$, which is dependent on the material specific Curie constant, $C = \mu_B\sqrt{\chi_M T}$, where χ_M is the molar magnetic susceptibility, T is the temperature in Kelvin and μ_B is the Bohr magneton.

Results and discussion

Single crystal diffractometry

Of the four paramagnetic ionic compounds discussed in this report, crystal structures are available for three of them, but not for $[bmim]^+/[FeCl_4]^-$. The $[N_{4444}]^+/[FeBrCl_3]^-$ crystal structure has been reported previously by Kruszyński and Wyrzykowski.[22] The most salient feature of the structure is that the iron–iron nearest neighbor spacings are 8.2 and 8.9 Å.

The structures of $[N_{1444}]^+/[FeCl_4]^-$ and $[Pyrr_{14}]^+/[FeCl_4]^-$ were solved and are illustrated in Fig. 2 and 3. The X-ray diffraction data for $[Pyrr_{14}]^+/[FeCl_4]^-$ are consistent with the hexagonal space group $P6_3mc$. The $[FeCl_4]^-$ anion has crystallographically imposed $3m$ symmetry. The disorder of the $[Pyrr_{14}]^+$ cation about the $(3)/m$ axis, a 3-fold axis intersecting with a mirror plane around the pyrrolidinium N atom,

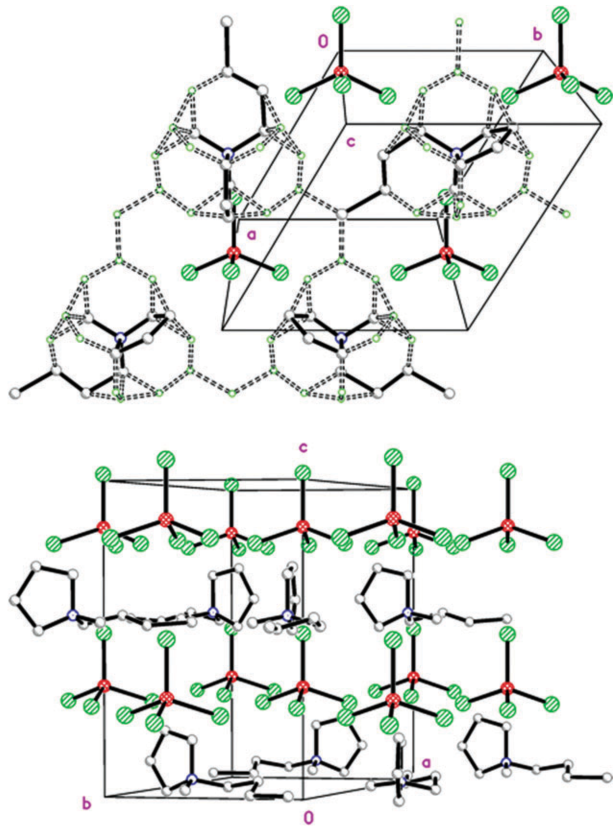

Fig. 2 Molecular packing of $[Pyrr_{14}]^+/[FeCl_4]^-$. (top) Orientation of this view is approximately 15 degrees offset from the crystallographic c-axis. The $[FeCl_4]^-$ anions are highly ordered, while the $[Pyrr_{14}]^+$ cations are disordered. An arbitrarily chosen $[Pyrr_{14}]^+$ conformation is indicated by the solid cation bonds; the remaining bonds in the disordered cation are shown by the open-dashed links. (bottom) This view is offset approximately 10 degrees from the diagonal between the crystallographic a and b axes. Site disordered atoms have been removed to illustrate one arbitrarily chosen cation per site.

is most likely due to the fragile glass forming nature of this ionic liquid. It is likely that these diffraction data result from

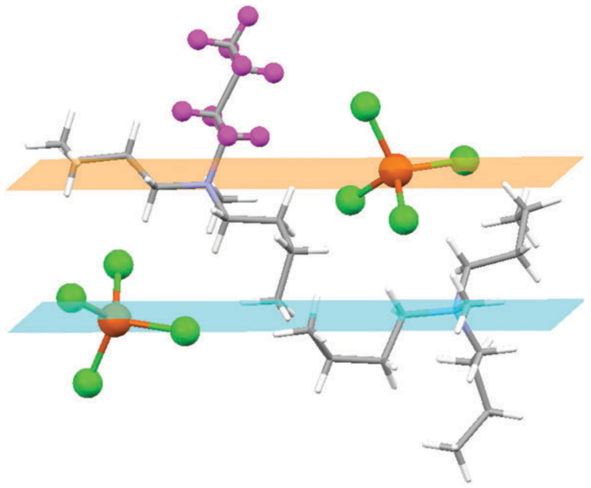

Fig. 3 Molecular packing of $[N_{1444}]^+/[FeCl_4]^-$. One-quarter of the total unit cell is shown. The orange and blue planes are orthogonal to the crystal *c*-axis. $[FeCl_4]^-$ anions are shown in ball-and-stick representation: iron atoms colored orange and chlorine atoms green. The lower $[N_{1444}]^+$ cation presents a propeller-like conformation with the three all-*gauche* butyl groups; the upper $[N_{1444}]^+$ cation shows one *trans* butyl group and two *gauche* butyl groups. The *trans* butyl group at top is labeled with magenta H atoms.

the presence of multiple low-energy crystal conformers. Because the crystal packing is determined by the tetrahalogenate anions, the butyl group on the $[Pyrr_{14}]^+$ cation fits into a three-fold symmetric site, leading to the observation of a crystal with ordered anions and three-fold disordered cations, as shown in Fig. 2 (top). Fig. 2 (bottom) illustrates that the crystal presents a layered structure, with an intra-layer iron–iron separation of 8.223(1) Å (the length of the *a*-axis) and an interlayer iron–iron spacing of 6.515(2) Å (half the length of the *c*-axis).

Examination of crystallographic data for tetramethyl- and tetraethyl-ammonium salts paired with small, symmetric metal halogenate anions shows that they all have layered structures.[17,23,27,28] The interlayer spacing between metal centers in these structures is typically 6.6 Å, with intralayer spacings between metals being typically 8.2 Å. Despite the length of the butyl group and quasi-rigid pyrrolidinium ring structure of $[Pyrr_{14}]^+$, our X-ray data for $[Pyrr_{14}]^+/[FeCl_4]^-$ shows that the crystal packing is quite similar to the tetramethylammonium[17] and tetraethylammonium[23,27] crystal structures, with interlayer metal spacing of 6.5 Å and intralayer metal atom spacings of 8.2 Å. All three structures show crystal packing in the $P6_3mc$ space group.

The structure of $[N_{1444}]^+/[FeCl_4]^-$ is shown in Fig. 3; for clarity, only one fourth of the unit cell is shown. The full unit cell with iron–iron distances labeled is shown in the Supplementary Information. The $[FeCl_4]^-$ anions are represented in ball-and-stick format with orange Fe(III) centers and Cl atoms colored green; the planes containing the $[FeCl_4]^-$ anions are parallel to the plane formed by the crystalline *a* and *b* axes and are colored orange and blue. The minimum iron–iron separation is 6.8 Å and the next near-neighbor distances range from 8.4 to 9.3 Å. The packing symmetry of the unit cell reveals two distinct conformations of the $[N_{1444}]^+$ cations. One $[N_{1444}]^+$ cation has butyl groups that each have gauche conformations, leading to a propeller-like structure for this ion. The other $[N_{1444}]^+$ cation has one *trans* butyl conformation and two *gauche* butyl groups. To highlight this structure, the *trans* butyl group has the hydrogens represented as magenta balls; these $[N_{1444}]^+$ cations project the *trans* butyl group above the top orange and blue planes that contain the $[FeCl_4]^-$ anions. The separations between cation hydrogen atoms and anion chlorine atoms all fall in the range between 2.8–3.0 Å.

Raman spectra

Vibrational Raman spectra of our four ionic compounds in the range 100–500 cm^{-1} show the previously observed symmetric Fe–Cl $T_d : A_1$ stretch at 331.9 ± 1.5 cm^{-1}.[11,29] This assignment provides further verification of the presence of the $[FeCl_4]^-$ anion. The 260 cm^{-1} Fe–Br stretching band ν_{Fe-Br} is observed in the $[N_{4444}]^+/[FeBrCl_3]^-$ spectrum confirming the presence of a single bromine in the anion.[30] Raman and FT-IR vibrational spectra of the four ionic compounds are available in the Supplementary Information.

Thermal properties

The thermal properties of $[N_{4444}]^+/[FeBrCl_3]^-$, $[Pyrr_{14}]^+/[FeCl_4]^-$ and $[N_{1444}]^+/[FeCl_4]^-$ were investigated by DSC. Prior to the first heating scan, the ionic compounds were cooled to either 143 or 153 K, and either two or three heat/cool cycles were scanned to reveal the details of intermediate, history-dependent phase behavior. The complete sets of DSC scans are shown in the Supplementary Information. Representative heating scans are depicted in Fig. 4. $[N_{4444}]^+/[FeBrCl_3]^-$ and $[N_{1444}]^+/[FeCl_4]^-$ cannot be classified as ionic liquids since they have melting points higher than 100 °C. $[N_{4444}]^+/[FeBrCl_3]^-$ exhibits a solid–solid transition at 379 K and a melting point at 409 K. Glass transitions were not observable for $[N_{4444}]^+/[FeBrCl_3]^-$ and $[N_{1444}]^+/[FeCl_4]^-$ because these salts crystallize easily upon cooling and are very difficult to quench as glasses. During the cooling process, $[N_{1444}]^+/[FeCl_4]^-$ crystallizes into a state that is metastable at lower temperatures, which upon heating anneals through an

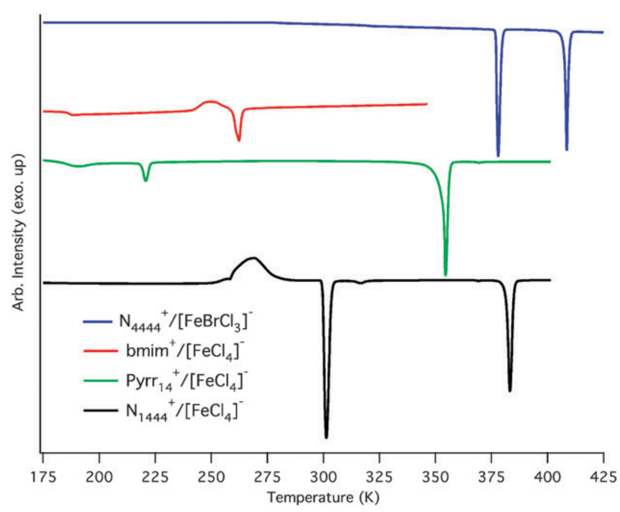

Fig. 4 DSC heat flow on warming for $[N_{4444}]^+/[FeBrCl_3]^-$, $[bmim]^+/[FeCl_4]^-$, $[Pyrr_{14}]^+/[FeCl_4]^-$ and $[N_{1444}]^+/[FeCl_4]^-$. Vertical offsets are 4, 2.5, 1.75 and 0 W/g, respectively.

exothermic process at 257 K. A transition between solid phases occurs at 301 K, a weak and history dependent annealing transition occurs at 317 K (approximately where $[N_{1444}]^+/[FeCl_4]^-$ undergoes snap crystallization when cooled) and a melting transition at 383 K. On the first scan of unmelted solid $[N_{1444}]^+/[FeCl_4]^-$, all of the previously-mentioned phase transitions are weak except for the melting transition at 383 K (see Supplementary Information). On a related note, the thermal properties of $[N_{4444}]^+/[FeCl_4]^-$ were reported by Wyrzykowski *et al.*; a solid–solid transition at 379 K preceded the melting transition at 409 K.[15]

We observed thermal behavior for $[bmim]^+/[FeCl_4]^-$ consistent with that reported previously by Yamamuro, *et al.*[13] On heating $[bmim]^+/[FeCl_4]^-$, we found a reproducible melting transition at 262 K, preceded by a cold crystallization at about 240 K. This confirms the classification of $[bmim]^+/[FeCl_4]^-$ as a room temperature ionic liquid, as opposed to being persistently supercooled, for example. The glass transition onset temperature of $[bmim]^+/[FeCl_4]^-$ is 189 K. Similar thermal properties are seen for $[Pyrr_{14}]^+/[FeCl_4]^-$, with a glass transition at 191 K, a solid–solid phase transition at 221 K and a melting point at 354 K, well above room temperature but still qualifying as an IL. Upon cooling, $[Pyrr_{14}]^+/[FeCl_4]^-$ recrystallizes abruptly between 350 and 342 K, and the solid–solid phase transition observed when heating is mirrored at 214 K in the cooling scans. Despite the existence of solid phases of $[Pyrr_{14}]^+/[FeCl_4]^-$ at low temperatures, there is enough disorder remaining to reveal the weak glass transition.

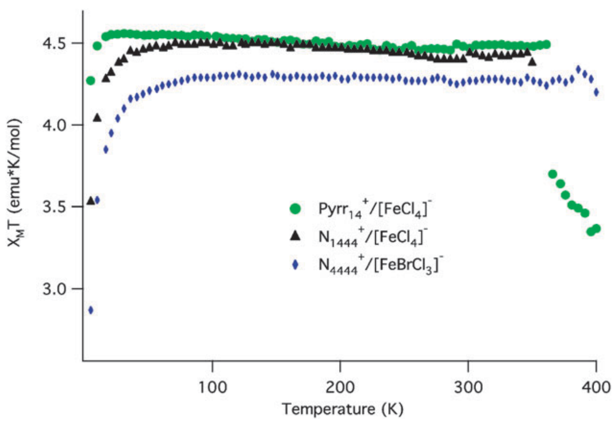

Fig. 5 $\chi_M T$ *vs.* temperature for $[Pyrr_{14}]^+/[FeCl_4]^-$, $[N_{1444}]^+/[FeCl_4]^-$ and $[N_{4444}]^+/[FeBrCl_3]^-$ for a heating and cooling rate of 5 K/min. Note that the sharp decrease in the value of $\chi_M T$ at 361 K for $[Pyrr_{14}]^+/[FeCl_4]^-$ results from melting of the sample.

Magnetic properties

Magnetic susceptibility measurements are plotted in Fig. 5 as $\chi_M T$ *vs.* temperature for $[N_{4444}]^+/[FeBrCl_3]^-$, $[N_{1444}]^+/[FeCl_4]^-$ and $[Pyrr_{14}]^+/[FeCl_4]^-$. Magnetic susceptibilities for the room-temperature IL $[bmim]^+/[FeCl_4]^-$ were previously reported by Hamaguchi *et al.*[10] and Yoshida *et al.*[8] and the magnetic properties of $[N_{4444}]^+/[FeBrCl_3]^-$ were reported in detail by Wyrzykowski *et al.*[17] All four compounds are paramagnetic at ambient temperatures. Paramagnetism is common in dilute transition-metal salts as the unpaired electrons interact weakly and their spins, which are randomly oriented at room temperature, align slightly in an external field. The Curie–Weiss Law (eqn (1)), was used to fit the data to find the material-dependent Curie and Weiss constants,

$$\chi = \frac{C}{T - \theta} \qquad (1)$$

where C is the Curie constant, T is the temperature in K and θ is the Weiss constant. Plots of $1/\chi_M$ *vs.* T show linear behavior over the entire range; these are presented in the Supplementary Information for $[N_{4444}]^+/[FeBrCl_3]^-$, $[Pyrr_{14}]^+/[FeCl_4]^-$ and $[N_{1444}]^+/[FeCl_4]^-$. The magnetic susceptibilities, effective magnetic moments and Curie constants are listed in Table 3. The calculated Weiss constants are close to zero within the experimental uncertainties, so we report only the Curie constants in Table 3, while the Weiss constants are included in the Supplementary Information. The effective magnetic moments have been calculated and are in agreement with the $S = 5/2$ high-spin electronic state of Fe(III) which has a spin-only value of 5.92 μ_B. Fig. 5 shows the product of molar susceptibility and temperature, $\chi_M T$, as a function of temperature. For clarity, only the heating curves are shown in Fig. 5 since the cooling curves are superposeable with the heating curves. In general, the $\chi_M T$ remains fairly constant over the temperatures investigated. The decrease in $\chi_M T$ for temperatures below 35 K for $[N_{1444}]^+/[FeCl_4]^-$ and $[N_{4444}]^+/[FeBrCl_3]^-$ is most significant for the latter compound. This drop in $\chi_M T$ with decreasing temperature is consistent with weakly antiferromagnetic behavior.[31] However, there are no deviations from monotonic behavior of $\chi_M T$ with decreasing temperature, indicating the absence of a Néel temperature. Minor bumps in the magnetic susceptibilities for the other salts correspond with phase transitions observed in the DSC data. $[N_{1444}]^+/[FeCl_4]^-$ has a transition at 301 K that is matched by a jump in the value of $\chi_M T$. DSC measurements of $[N_{4444}]^+/[FeBrCl_3]^-$ show a solid–solid phase transition onset temperature at 379 K that corresponds with the increase in $\chi_M T$ observed near 381 K. The values we obtain for $[N_{4444}]^+/[FeBrCl_3]^-$ are

Table 2 DSC transition temperatures in K. Peak values are reported for the melting transitions, while all others are reported as onset temperatures. Transition enthalpies are listed in parentheses (in kJ/mol) in the columns for $T_{s\text{–}s}$ and T_m

Cation	Anion	T_g	$T_{cold\text{–}cryst/anneal}$	$T_{s\text{–}s}$ [a]	T_{anneal}	T_m
$[N_{4444}]^+$	$[FeBrCl_3]^-$	—	—	379 (15.7)	—	409 (13.8)
$[bmim]^+$	$[FeCl_4]^-$	189	240	—	—	262 (4.38)
$[Pyrr_{14}]^+$	$[FeCl_4]^-$	191	—	221	—	354 (15.6)
$[N_{1444}]^+$	$[FeCl_4]^-$	—	257	301 (19.7)	317	383 (17.0)

[a] Transition between two solid phases.

Table 3 Magnetic properties of $[N_{1444}]^+/[FeCl_4]^-$ (FW = 398.0 g/mol), $[Pyrr_{14}]^+/[FeCl_4]^-$ (FW = 339.9 g/mol) and $[N_{4444}]^+/[FeBrCl_3]^-$ (FW = 484.6 g/mol)

Compound	$[N_{1444}]^+/[FeCl_4]^-$	$[Pyrr_{14}]^+/[FeCl_4]^-$	$[bmim]^+/[FeCl_4]^-$	$[N_{4444}]^+/[FeBrCl_3]^-$
Curie Const. (emu-K/mol)	4.41	4.47	—	4.28 (5.06[c])
μ_{eff} (μ_B)	5.29	5.98	5.82[a]	5.85
At 300 K:				
$\chi_M T$ (emu-K/mol)	4.42	4.47	4.11[b]	4.27 (4.95[c])
μ_{eff} (μ_B)	5.95	5.98	5.73[b]	5.84 (6.29[c])
At 100 K:				
$\chi_M T$ (emu-K/mol)	4.49	4.54	—	4.26
μ_{eff} (μ_B)	5.99	6.03	—	5.84
At 5 K:				
$\chi_M T$ (emu-K/mol)	3.53	4.27	—	2.81
μ_{eff} (μ_B)	5.31	5.84	—	4.79

[a] Values from Yoshida *et al.*[8] [b] χ_M value at 300 K from Hayashi, *et al.*[11] used to calculate $\chi_M T$ and μ_{eff}. [c] Values obtained using a 0.5 T external magnetic field by Wyrzykowski *et al.*[32]

in good agreement with those previously reported by Wyrzykowski *et al.*[32]

Conclusions

Four paramagnetic ionic compounds have been prepared: $[Pyrr_{14}]^+/[FeCl_4]^-$, $[N_{1444}]^+/[FeCl_4]^-$, $[N_{4444}]^+/[FeBrCl_3]^-$ and $[bmim]^+/[FeCl_4]^-$; the synthesis and characterization of the first two are reported here for the first time. While only $[bmim]^+/[FeCl_4]^-$ is liquid at ambient temperatures, $[Pyrr_{14}]^+/[FeCl_4]^-$ qualifies as an ionic liquid with a melting point of 355 K. Though $[bmim]^+/[FeCl_4]^-$ and $[Pyrr_{14}]^+/[FeCl_4]^-$ have T_g values of 189 and 191 K, respectively, the melting temperature of the latter is 92 K above that of the former.

Paramagnetism in these ionic liquids and solids results from the Fe(III)-containing anions. At the lowest temperatures between 5 to 35 K, the drop in the value of $\chi_M T$ is consistent with weak antiferromagnetism that has been observed by Wyrzykowski and co-workers in related compounds.

X-ray diffraction results provide structures of the two new compounds $[Pyrr_{14}]^+/[FeCl_4]^-$ and $[N_{1444}]^+/[FeCl_4]^-$. The $[Pyrr_{14}]^+/[FeCl_4]^-$ structure shows a highly ordered hexagonal lattice for the $[FeCl_4]^-$ anions, but three-fold orientational disorder for the $[Pyrr_{14}]^+$ cations. The orthorhombic crystal structure found for $[N_{1444}]^+/[FeCl_4]^-$ shows that each of the two unique cations in the unit cell have different conformations of the butyl groups.

These and related paramagnetic ionic liquids and solids may provide the basis for strongly paramagnetic media that can exist in crystal, vitreous, liquid or solution conditions. Such paramagnetic and ionic media will likely find applications in separations chemistry, catalysis, and nanotechnology. In particular, $[FeCl_4]^-$ ionic liquids seem well positioned for use as alternatives for $FeCl_3$ in Friedel–Crafts or Grignard reactions.

Acknowledgements

We thank our colleagues Prof. Gene S. Hall for Raman and FT-IR spectra, Dr. Viktor Poltavets and Prof. Martha Greenblatt for SQUID magnetometer measurements, and Dr. Ashley L. Carbone and Prof. Kathryn E. Uhrich for use of their DSC instrumentation.

BMK thanks Douglass College and the Rutgers Aresty Research Center for Undergraduates for funding. We gratefully acknowledge support for this work from the National Science Foundation and the Department of Energy. Work done at Rutgers was supported by National Science Foundation grant number CHE-0718391. Work at Brookhaven was supported under Contract No. DE-AC02-98CH10886 with the US Department of Energy and supported by its Division of Chemical Sciences, Geosciences and Biosciences, Office of Basic Energy Sciences.

References

1 N. V. Plechkova and K. R. Seddon, *Chem. Soc. Rev.*, 2008, **37**, 123–150.
2 C. Guerrero-Sanchez, T. Lara-Ceniceros, E. Jiminez-Regalado, M. Rasa and U. S. Schubert, *Adv. Mater.*, 2007, **19**, 1740–1747.
3 H. Morimoto, T. Ukai, Y. Nagaoka, N. Grobert and T. Maekawa, *Physical Review E*, 2008, **78**, 021403-1–021403-7.
4 F. C. C. Oliveira, L. M. Rossi, R. F. Jardim and J. C. Rubim, *J. Phys. Chem. C*, 2009, **113**, 8566–8572.
5 G. Clavel, J. Larionova, Y. Guari and C. Guérin, *Chem.–Eur. J.*, 2006, **12**, 3798–3804.
6 K. Bica and P. Gaertner, *Org. Lett.*, 2006, **8**(4), 733–735.
7 G. Wang, N. Yu, L. Peng, R. Tan, H. Zhao, D. Yin, H. Qiu, Z. Fu and D. Yin, *Catal. Lett.*, 2008, **123**, 252–258.
8 Y. Yoshida, A. Otsuka, G. Saito, S. Natsume, E. Nishibori, M. Takata, M. Sakata, M. Takahashi and T. Yoko, *Bull. Chem. Soc. Jpn.*, 2005, **78**, 1921–1928.
9 Y. Yoshida and G. Saito, *J. Mater. Chem.*, 2006, **16**, 1254–1262.
10 S. Hayashi and H.-o. Hamaguchi, *Chem. Lett.*, 2004, **33**, 1590–1591.
11 S. Hayashi, S. Saha and H.-o. Hamaguchi, *IEEE Trans. Magn.*, 2006, **42**, 12–14.
12 M. Okuno, H. Hamaguchi and S. Hayashi, *Appl. Phys. Lett.*, 2006, **89**, 132506.
13 O. Yamamuro, Y. Inamura, S. Hayashi and H.-o. Hamaguchi, in *CP832, Flow Dynamics, The Second International Conference on Flow Dynamics*, ed. M. Tokuyama and S. Maruyama, American Institute of Physics, 2006, vol. 832 of AIP Conference Proceedings, pp. 73–80.
14 A. P. Abbott, G. Capper, D. L. Davies and R. Rasheed, *Inorg. Chem.*, 2004, **43**, 3447–3452.

15 D. Wyrzykowski, T. Maniecki, A. Pattek-Janczyk, J. Stanek and Z. Warnke, *Thermochim. Acta*, 2005, **435**, 92–98.
16 D. Wyrzykowski, R. Kruszyński, T. Maniecki and Z. Warnke, *Journal of Inorganic and General Chemistry*, 2007, **633**, 285–289.
17 D. Wyrzykowski, R. Kruszyński, J. Mroziński and Z. Warnke, *Inorg. Chim. Acta*, 2008, **361**, 262–268.
18 R. E. Del Sesto, T. M. McCleskey, A. K. Burrell, G. A. Baker, J. D. Thompson, B. L. Scott, J. S. Wilkes and P. Williams, *Chem. Commun.*, 2008, 447–449.
19 S. A. Kozlova, S. P. Verevkin, A. Heintz, T. Peppel and M. Kockerling, *J. Chem. Eng. Data*, 2009, **54**(5), 1524–1528.
20 B. Mallick, B. Balke, C. Felser and A.-V. Mudring, *Angew. Chem., Int. Ed.*, 2008, **47**(40), 7635–7638.
21 S. Tang, A. Babai and A.-V. Mudring, *Angew. Chem., Int. Ed.*, 2008, **47**(40), 7631–7634.
22 R. Kruszyński and D. Wyrzykowski, *Acta Crystallogr., Sect.E: Struct. Rep. Online*, 2006, **62**, m994–m996.
23 D. J. Evans, A. Hills, D. L. Hughes and G. J. Leigh, *Acta Crystallogr., Sect. C: Cryst. Struct. Commun.*, 1990, **46**, 1818–1821.
24 M. T. Hay and S. J. Geib, *Acta Crystallogr., Sect. E: Struct. Rep. Online*, 2005, **E61**, m190–m191.
25 SADABS, Bruker Nonius Area Dector Scaling and Absorption Correction. Bruker-AXS.; Bruker-AXS Inc., 2003.
26 G. M. Sheldrick, *Acta Crystallogr., Sect. A: Found. Crystallogr.*, 2008, **64**(1), 112–122.
27 J. Trotter, F. W. B. Einstein and D. G. Tuck, *Acta Crystallogr., Sect. B: Struct. Crystallogr. Cryst. Chem.*, 1969, **25**, 603–604.
28 M. Lenck, S. Dou and A. Weiss, *Zeitschrift fur Naturforschung Section A—A Journal of Physical Sciences (Z.Naturforsch., A: Phys.Sci.)*, 1991, **46**, 777–784.
29 M. S. Sitze, E. R. Schreiter, E. V. Patterson and R. G. Freeman, *Inorg. Chem.*, 2001, **40**, 2298–2304.
30 S. K. Jain, B. S. Garg and Y. K. Bhoon, *Transition Met. Chem.*, 1986, **11**, 89–95.
31 A. Wold and K. Dwight, *Solid State Chemistry: Synthesis, Structure, and Properties of Selected Oxides and Sulfides*, Chapman & Hall, New York, 1993.
32 D. Wyrzykowski, R. Kruszyński, J. Kak, J. Mroziński and Z. Z. Warnke, *Z. Anorg. Allg. Chem.*, 2007, **633**, 2071–2076.